Supporting Information

Confining an Ag_{10} Core in an Ag_{12} Shell: A Four-Electron Superatom with Enhanced Photoluminescence upon Crystallization

Esma Khatun,[a] Mohammad Bodiuzzaman,[a] Korath Shivan Sugi,[a] Papri Chakraborty,[a] Ganesan Paramasivam,[a] Wakeel Ahmed Dar,[a] Tripti Ahuja,[a] Sudhadevi Antharjanam[b] and Thalappil Pradeep[a]*

a. Department of Chemistry, DST Unit of Nanoscience (DST UNS) and Thematic Unit of Excellence (TUE), Indian Institute of Technology Madras, Chennai 600036, India.

b. Sophisticated Analytical Instruments Facility, Indian Institute of Technology Madras, Chennai 600036, India.

E-mail: pradeep@iitm.ac.in

Table of contents

Crystallographic analysis

X-ray data collection was performed with Bruker AXS Kappa Apex III CMOS Diffractometer equipped with graphite monochromated Mo (K_α) (λ = 0.71073 Å) radiation at 273K. The automatic cell determination routine, with 24 frames at two different orientations of the detector was employed to collect reflections for unit cell determination. Further, intensity data for structure determination were collected through an optimized strategy which gave an average 4-fold redundancy. The program APEX3-SAINT (Bruker, 2016) was used for integrating the frames. Four-fold redundancy per reflection was utilized for achieving good multi-scan absorption correction using the program SADABS (Bruker, 2016). The structure was solved by SHELXT-2014 (Sheldrick, 2014) and refined by full-matrix least squares techniques using the same program. Hydrogens on all carbon atoms were fixed at calculated positions and refined as riding model with C—H = 0.93 Å (C-H = 0.96 Å for CH_3), Uiso(H) = 1.2Ueq(C) (Uiso(H) = 1.5Ueq(C) for CH_3). The molecule is crystallized in body-centered tetragonal crystal system with I4(1)/a space group. The asymmetric unit contains one-fourth of the silver cluster with one silver atom (Ag_3) at the 4-fold axis of symmetry. Solvent and counter

ions were not modeled due to difficulty in locating and refining their positions satisfactorily. One of the 2,5-DMBT moieties is disordered by 180° rotation through the S2-C43 bond over two positions with a site-occupancy ratio of 60:40. The disorder was resolved by successive Fourier electron density maps and least squares refinements. Sum of the occupancies of the disordered components was restrained as 1 during refinement. The corresponding bond distances of disordered groups were restrained to be equal within an allowed standard deviation of 0.02 Å. Similar restraints were applied to the thermal parameters of the disordered components of the molecule. Thermal parameters of the atoms of the moiety were restrained to show approximate isotropic behaviour within an effective standard deviation of 0.02 Å.

Crystal Information

Table S1. Crystal data and structure refinement for $[Ag_{22}(dppe)_4(2,5\text{-}DMBT)_{12}Cl_4]^{2+}$.

Identification code	ag22	
Empirical formula	C200 H204 Ag22 Cl4 P8 S12	
Formula weight	5755.04	
Temperature	273(2) K	
Wavelength	0.71073 Å	
Crystal system	Tetragonal	
Space group	$I4_1/a$	
Unit cell dimensions	a = 19.4007(9) Å	a= 90°.
	b = 19.4007(9) Å	b= 90°.
	c = 57.9021(18) Å	g = 90°.
Volume	21794(2) $Å^3$	
Z	4	
Density (calculated)	1.754 Mg/m^3	
Absorption coefficient	2.194 mm^{-1}	
F(000)	11272.0	
Crystal size	0.250 x 0.200 x 0.150 mm^3	
Theta range for data collection	2.934 to 20.864°.	
Index ranges	-19<=h<=19, -19<=k<=19, -57<=l<=57	
Reflections collected	42397	
Independent reflections	5629 [R(int) = 0.0718]	

Completeness to theta = 20.864°	97.7 %
Absorption correction	Semi-empirical from equivalents
Max. and min. transmission	0.7446 and 0.5734
Refinement method	Full-matrix least-squares on F^2
Data / restraints / parameters	5629 / 311 / 628
Goodness-of-fit on F^2	1.135
Final R indices [I>2sigma(I)]	R1 = 0.1267, wR2 = 0.2562
R indices (all data)	R1 = 0.1950, wR2 = 0.3121
Extinction coefficient	n/a
Largest diff. peak and hole	1.467 and -1.525 e.$Å^{-3}$

Supporting information 1

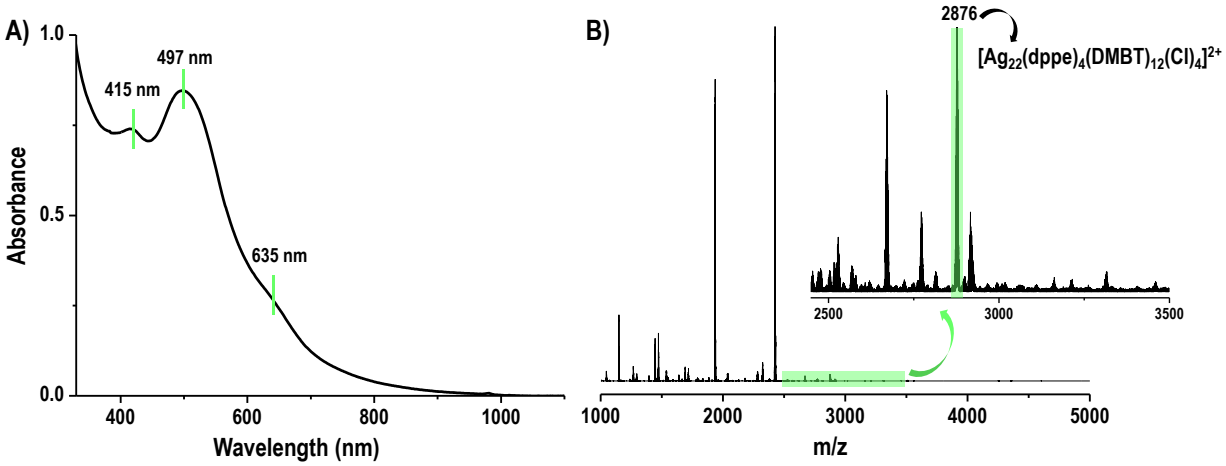

Figure S1. (A) UV-vis absorption spectrum and (B) HRESI MS of $[Ag_{22}(dppe)_4(2,5\text{-}DMBT)_{12}Cl_4]^{2+}$ before size focusing. The absorption spectrum of the crude product shows two features at ~415 and 497 nm along with a small hump at 635 nm. The feature at m/z 2876 is due to $[Ag_{22}(dppe)_4(2,5\text{-}DMBT)_{12}Cl_4]^{2+}$.

Supporting information 2

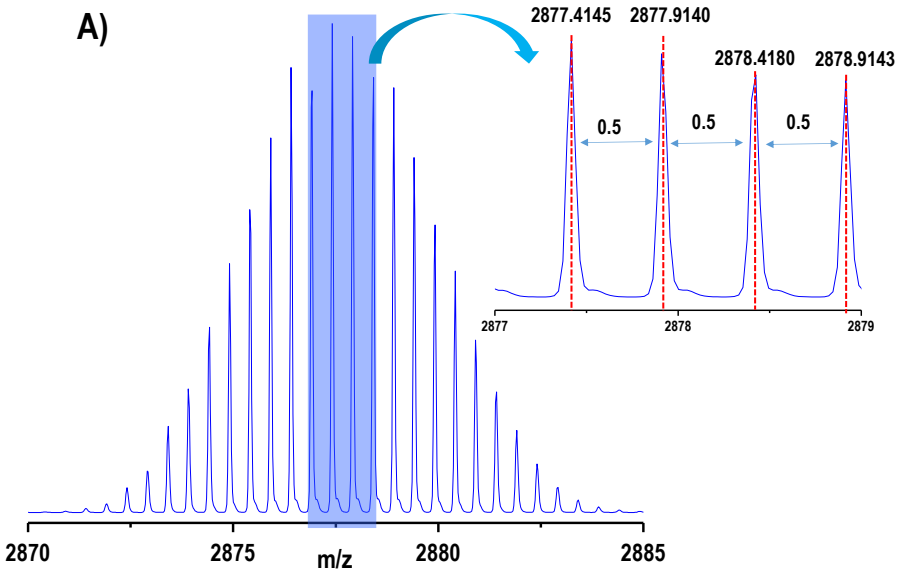

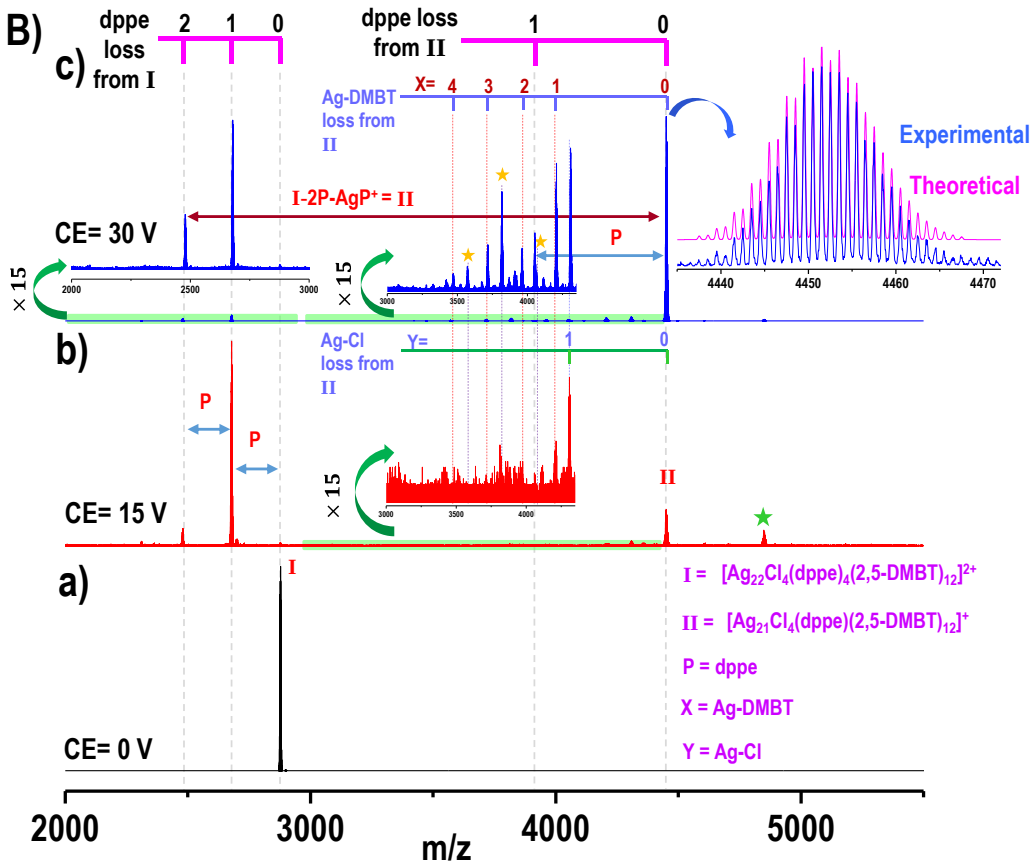

Figure S2. (A) Expanded view of the peak at m/z 2876. Separation between two successive peaks is 0.5 which confirms the 2^+ charge state. (B) Collision-induced dissociation (CID) mass spectrum of the peak at 2876 which is assigned as $[Ag_{22}(dppe)_4(2,5\text{-}DMBT)_{12}Cl_4]^{2+}$ (panel a). It shows systematic loss of four dppe ligands upon increase in collision energy along with the loss of some Ag-DMBT and AgCl units. Various species involved are marked in the inset of panel a. After the loss of one Ag-Cl from **II** (panel b), the formed species undergoes systematic Ag-DMBT losses which are denoted by yellow asterisks (panel c). The peak marked with green asterisk in panel b is assigned as $[Ag_{21}(dppe)_2(2,5\text{-}DMBT)_{12}Cl_4]^{+}$. Theoretical and experimental isotopic distributions of **II** are expanded in the inset of panel c.

Supporting information 3:

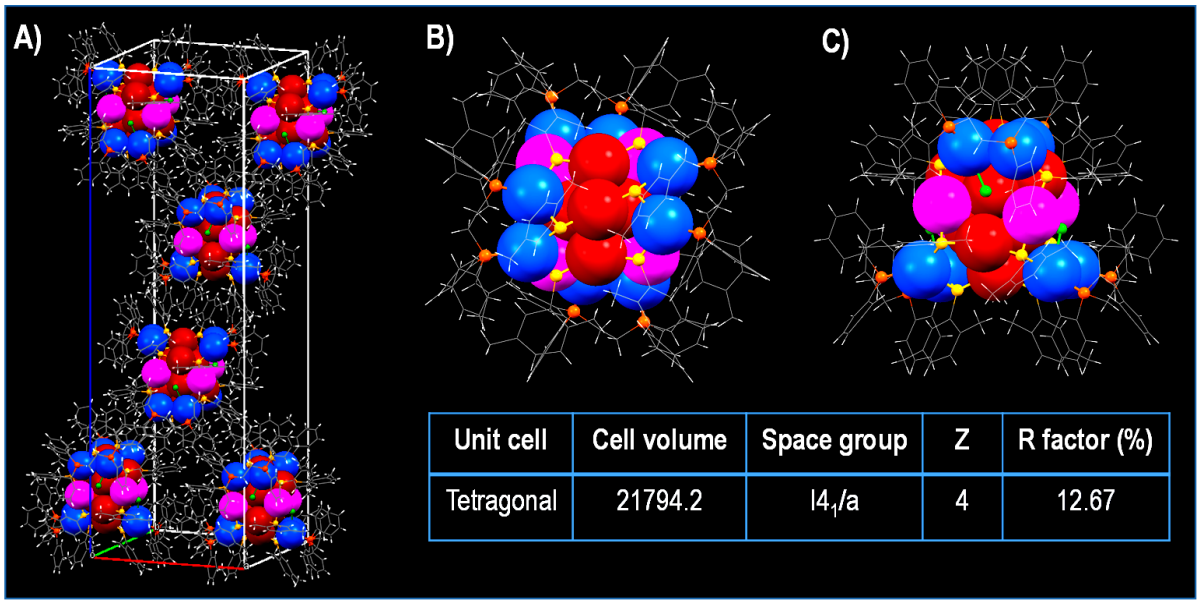

Figure S3. The overall structure of $[Ag_{22}(dppe)_4(2,5\text{-}DMBT)_{12}Cl_4]^{2+}$: A) Unit cell with a tetragonal arrangement; B) top view; C) side view. Labels: red, blue and pink = Ag, yellow = S, orange = P, green = Cl, gray = C and white = H.

Supporting information 4

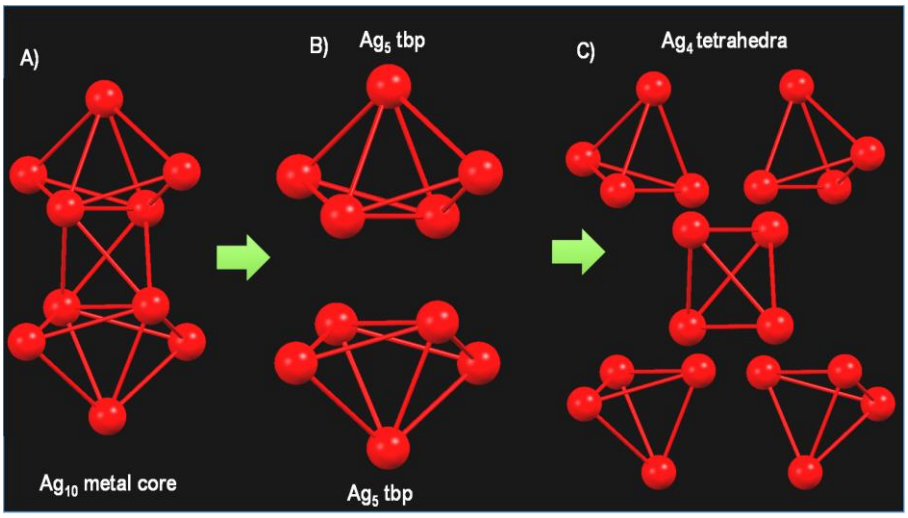

Figure S4. Anatomy of the Ag_{10} core: (A) Ag_{10} core, (B) Ag_{10} is composed of two perpendicular Ag_5 units having trigonal bipyramidal (tbp) geometry, (C) Ag_{10} can also be viewed as a combination of five edge and face shared Ag_4 tetrahedra.

Supporting information 5

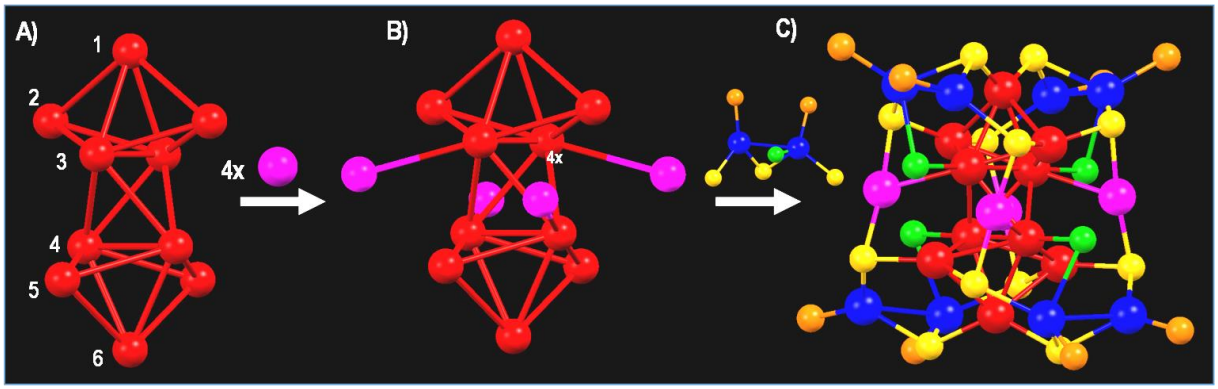

Figure S5. (A) Ag_{10} metal core, (B) Ag_{14} unit, (C) $Ag_{22}P_8S_{12}Cl_4$.

The shell is formed by four $Ag_2S_3P_2Cl$ and four Ag atoms. Out of the four $Ag_2S_3P_2Cl$ staples, two connect the first three layers of the core and remaining two connect the last three layers perpendicularly. The remaining four silver atoms are connected with the third and fourth layer

of the Ag_{10} core and also act as bridging atoms between the $Ag_2S_3P_2Cl$ staples of the first three and the last three layers.

Labels: red, blue and pink = Ag, yellow = S, orange = P, green = Cl, C and H atoms are omitted here for clarity.

Supporting information 6

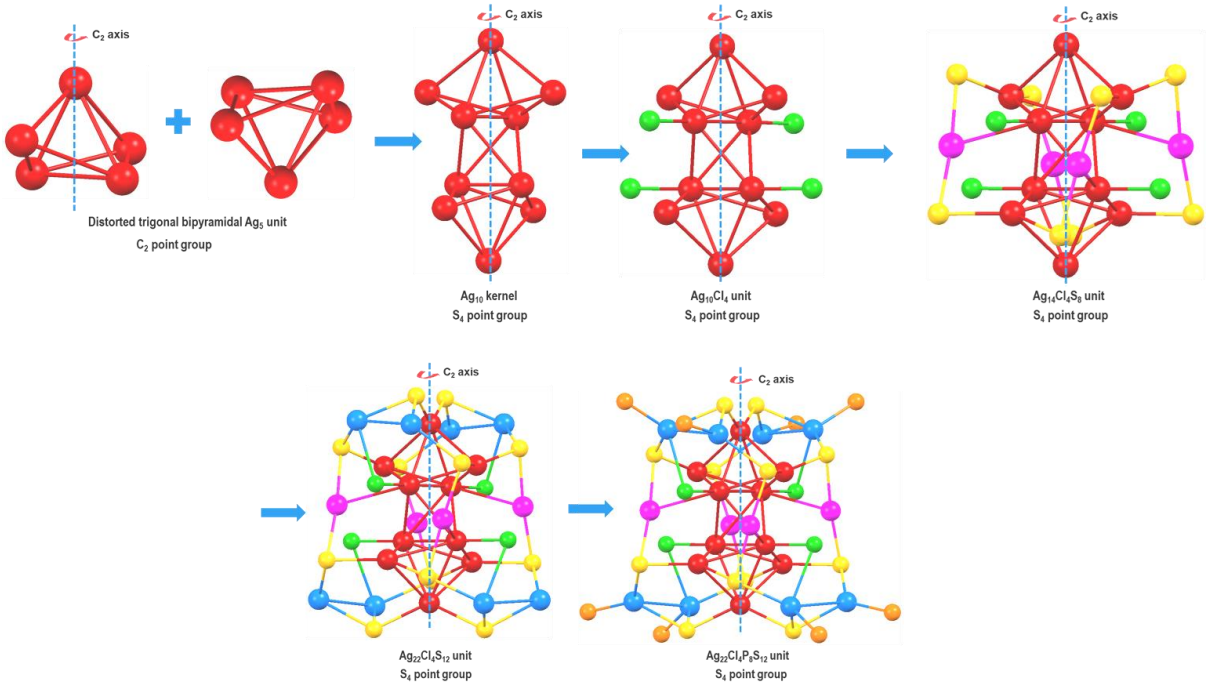

Figure S6. Symmetry and orientations in $[Ag_{22}(dppe)_4(2,5\text{-}DMBT)_{12}Cl_4]^{2+}$. The Ag_5 units possess a chiral C_2 point group while the Ag_{10} core unveils an achiral S_4 point group. Staples are connected to the core in such a way that S_4 symmetry is maintained. Labels: red, blue and pink = Ag, yellow = S, orange = P, green = Cl. C and H atoms are omitted here for clarity.

Table S2. A list of reported silver nanoclusters having crystal structures.

Cluster composition	Inner core	Shell	Unit cell	Nominal electron count	References
$[Ag_{14}(DFBT)_{12}(PPh_3)_8]$	Ag_6 (octahedron)	$Ag_8S_{12}P_8$	Primitive	2	1
$[Ag_{15}(N\text{-}triphos)_4(Cl_4)]^{3+}$	Ag_9 (centered cube)	$Ag_6N_4P_{12}Cl_4$	C2221 Orthorhombic	8	2
$[Ag_{16}(DPPE)_4(DFBT)_{14}]$	Ag_8 (Ag_4 rhombus capped by Ag_2 unit)	$Ag_8P_8S_{14}$	I 4_1/a Tetragonal	2	3
$[Ag_{21}[S_2P(O^iPr)_2]_{12}]^+$	Ag_{13} (centered icosahedron)	$Ag_8S_{24}P_{12}$	$P2_1$/n Monoclinic	8	4
$[Ag_{23}(PET)_{18}(PPh_3)_8]$	Ag_{12} (two connected rhombic bipyramidal	$Ag_{12}S_{18}P_8$	Cc Monoclinic	5	5
$[Ag_{25}(DMBT)_{18}]^-$	Ag_{13} (centered icosahedra)	$Ag_{12}S_{18}$	P-1 Triclinic	8	6
$[Ag_{29}(BDT)_{12}(PPh_3)_4]^{3-}$	Ag_{13} (centered icosahedra)	$Ag_{16}S_{24}P_8$	Pa-3 Cubic	8	7
$[Ag_{32}(DPPE)_5(SC_6H_3F_2)_{24}]^{2-}$	Ag_{22} (pentagon face-sharing bi-pentagonal antiprism)	$Ag_{10}P_{10}S_{24}$	C 2/c Monoclinic	10	3
$[Ag_{32}(Dppm)_5(SAdm)_{13}Cl_8]^{3+}$	Ag_{13} (centered icosahedra)	$Ag_{19}P_{10}S_{13}Cl_8$	P-1 Triclinic	8	8
$[Ag_{35}(H_2L)_2(L)(C{\equiv}{\equiv}CBu^t)_{16}]^{3+}$	Ag_{13} (centered icosahedra)	$Ag_{22}S_{12}(C{\equiv}{\equiv}CBu^t)_{16}$	P-1 Triclinic	8	9
$[Ag_{38}(SPhF_2)_{26}(PPh_3)_8$	Ag_{14} (fcc)	$Ag_{24}S_{26}P_8$	P-1 Triclinic	12	10
$[Ag_{40}(SPhMe_2)_{24}(PPh_3)_8]^{2+}$	Ag_8 (cube)	$Ag_{32}S_{24}P_8$	C2/m Monoclinic	14	11
$[Ag_{44}(FTP)_{30}]^{4-}$	Ag_{12} (hollow icosahedra)	$Ag_{32}S_{30}$	P-1 Triclinic	18	12
$[Ag_{45}(Dppm)_4(SAdm)_{16}Br_{12}]^{3+}$	Ag_{23} (face shared biicosahedra)	$Ag_{22}S_{16}P_8Br_{12}$	C12/c1 Monoclinic	14	8
$[Ag_{46}(SPhMe_2)_{24}(PPh_3)_8]^{2+}$	Ag_{14} (fcc)	$Ag_{32}S_{24}P_8$	C2/m Monoclinic	20	11
$Ag_{50}(DPPM)_6(TBBM)_{30}$	Ag_{12} (hollow icosahedra)	$Ag_{38}S_{30}P6$	P-1 Triclinic	20	13
$[Ag_{62}(S^tBu)_{32}S_{12}]^{2+}$	Ag_{14} (fcc)	$Ag_{48}S_{44}$	P-1 Triclinic	4*	14

$[Ag_{63}(SPhF_2)_{36}(PR'_3)_8]^+$	Ag_{14} (fcc)	$Ag_{49}S_{36}P_8$	R-3 Trigonal	26	10
$[Ag_{67}(SPhMe_2)_{32}(PPh_3)_8]^{3+}$	Ag_{23} (centred cuboctahedra)	$Ag_{44}S_{32}P_8$	Ccc2 Orthorhombic	32	15
$[Ag_{78}(BDPP)_6(SR)_{42}]$	Ag_{22} (three mutually interpenetrating icosahedra)	$Ag_{56}S_{42}P_6$	Ccc2 Orthorhombic	36	16
$[Ag_{141}X_{12}(SAdm)_{40}]^{3+}$ (X=Cl, Br, I)	Ag_{19} (interpenetrating biicosahedra)	$Ag_{122}S_{40}X_{12}$	Pbcn Orthorhombic	86	17
$[Ag_{136}(SR)_{64}Cl_3Ag_{0.45}]^-$	Ag_{54} (pentagonal bipyramids)	$Ag_{82}S_{64}$	P-1 Triclinic	70	18
$Ag_{374}(SR)_{113}Br_2Cl_2$	Ag_{207} (elongated pentagonal bipyramids)	$Ag_{167}S_{113}Br_2Cl_2$	R-3c rhombohedral	257	18
$[Ag_{22}(dppe)_4(DMBT)_{12}Cl_4]^{2+}$	Ag_{10} (two tbp units connected to each other perpendicularly)	$Ag_{12}S_{12}P_8Cl_4$	$I4_1/a$ Tetragonal	4	

*Although the nominal electron count is 4, the superatom electron count calculated is 2.[14]

Acronyms of ligands used:

DFBT: 3,4-difluoro-benzenethiol

N-triphos: tris((diphe- nylphosphino)methyl)amine)

DPPE: 1,2-bis(diphenylphosphino)ethane

PET: 2-phenylethanethiol

DMBT: 2,4-dimethylbenzenethiol

BDT: 1,3-benzenedithiol

Dppm: 1,1-bis(diphenylphosphino)methane

H_4L: p-tert-butylthiacalix[4]-arene

FTP: 4-fluorothiophenol

SAdm: Adamentanethiol

S^tBu: tert-butylbenzenethiol

BDPP: 2,4-bis(diphenylphosphino)pentane

TBBM: 4-tert-butylbenzylmercaptant

Supporting information 7

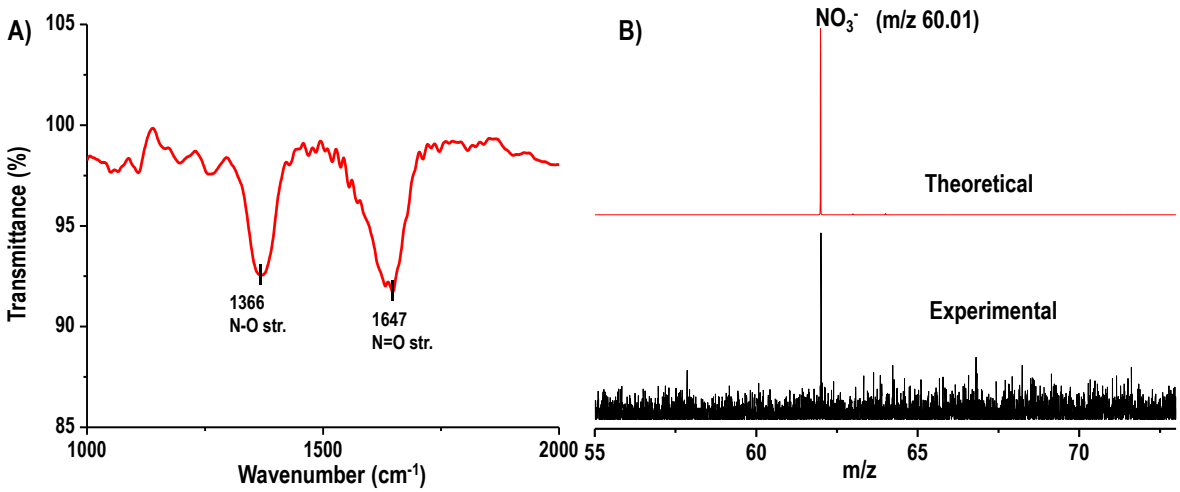

Figure S7. (A) IR spectrum of $[Ag_{22}(dppe)_4(2,5\text{-}DMBT)_{12}Cl_4]^{2+}$ which shows two peaks corresponds to N-O stretching and N=O stretching frequencies. (B) HRESI MS of $[Ag_{22}(dppe)_4(2,5\text{-}DMBT)_{12}Cl_4]^{2+}$ shows peak corresponding to NO_3^-. These two experiments confirm the presence of NO_3^- as the counterion.

Supporting information 8

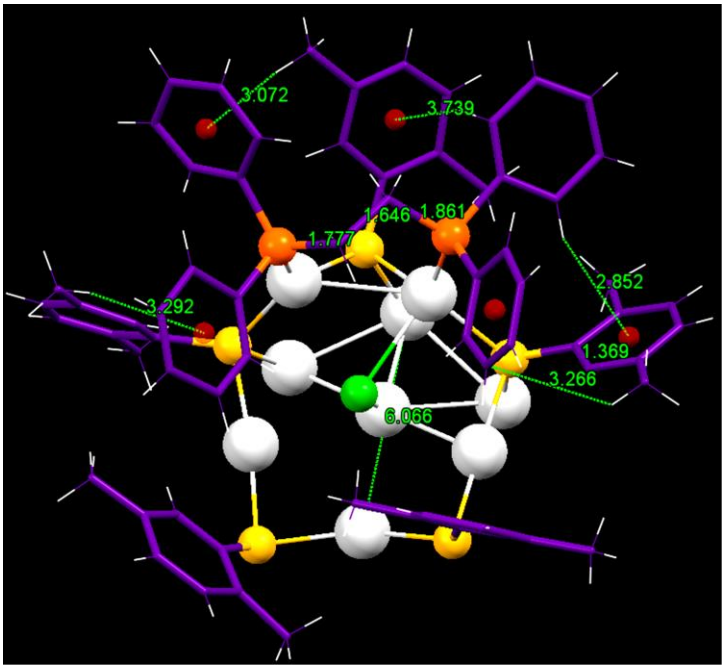

Figure S8. C-H… π interactions between benzene rings of dppe and 2,5-DMBT.

Supporting information 9

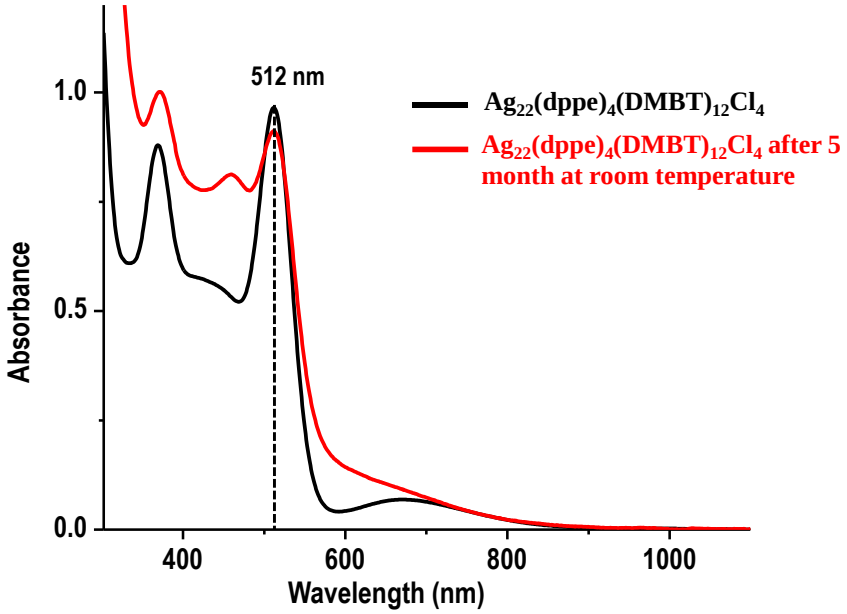

Figure S9. Time-dependent absorption spectra of $[Ag_{22}(dppe)_4(2,5\text{-}DMBT)_{12}Cl_4]^{2+}$ at room temperature. The absorption features are similar in both the spectra after 5 months at room temperature which suggest the stability of the cluster.

Supporting information 10

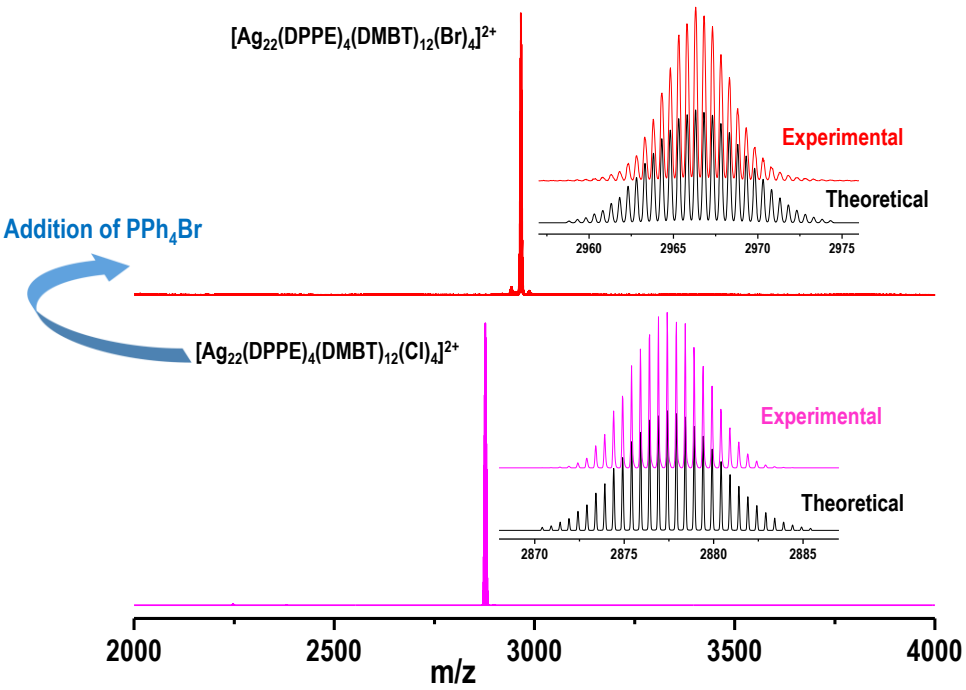

Figure S10. Replacement of Cl^- by Br^- using PPh_4Br. The lower panel shows the ESI MS of $[Ag_{22}(dppe)_4(2,5\text{-}DMBT)_{12}Cl_4]^{2+}$ and upper panel corresponds to the ESI MS of Br substituted product, $[Ag_{22}(dppe)_4(DMBT)_{12}Cl_{4-n}Br_n]^{2+}$ where n=0-4.

Supporting information 11

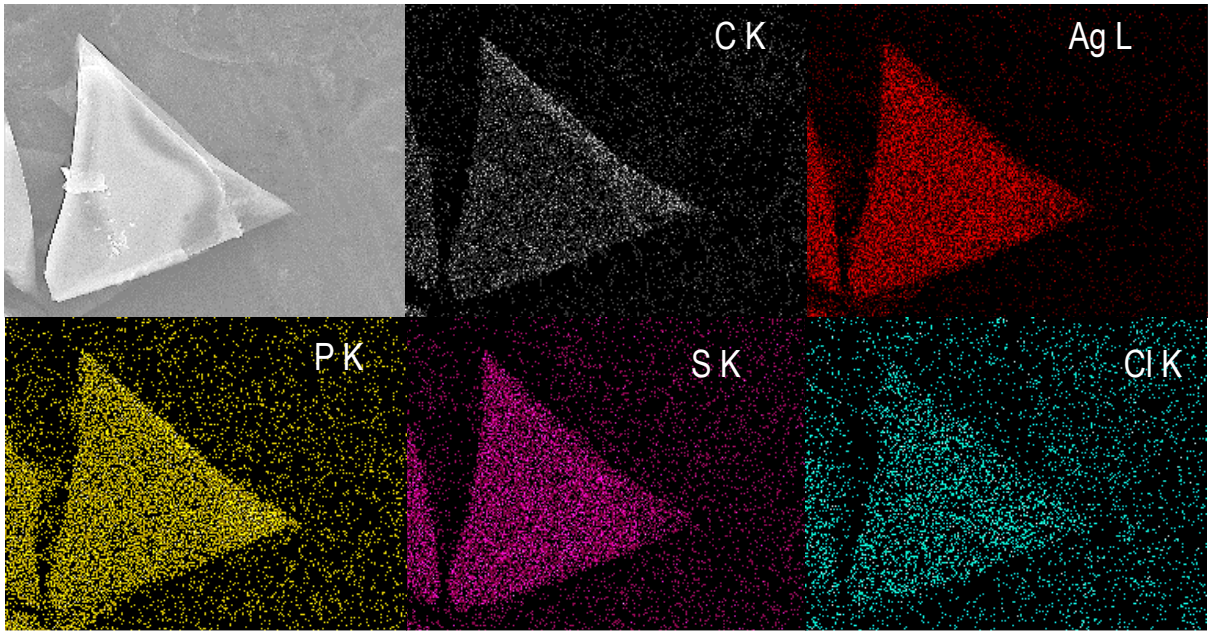

Figure S11. SEM image and EDS mapping of $[Ag_{22}(dppe)_4(2,5\text{-}DMBT)_{12}Cl_4]^{2+}$. C, Ag, P, S and Cl are represented by white, red, yellow, purple and light blue colors, respectively.

Supporting information 12

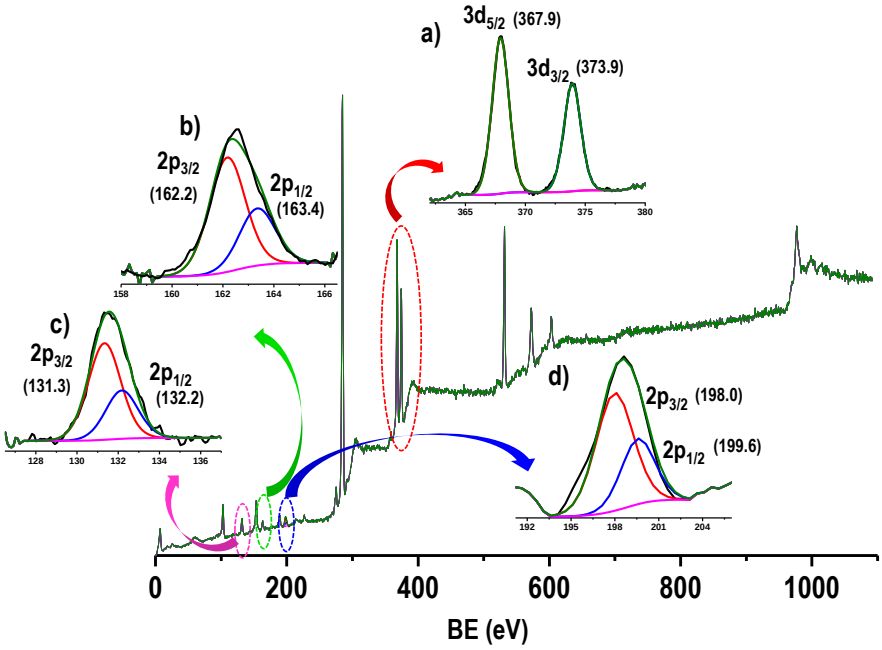

Figure S12. XPS spectrum of $[Ag_{22}(dppe)_4(2,5\text{-}DMBT)_{12}Cl_4]^{2+}$. Expanded area of (a) Ag 3d, (b) S 2p, (c) P 2p and (d) Cl 2p.

Supporting information 13

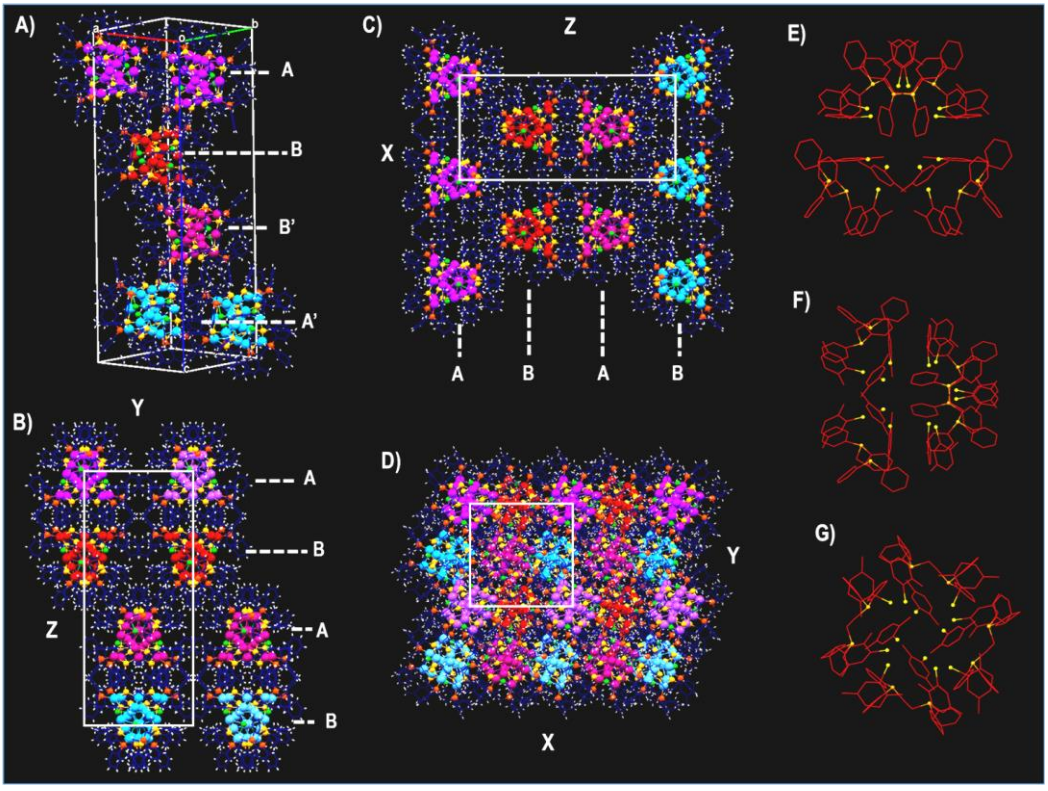

Figure S13. Packing diagram of $[Ag_{22}(dppe)_4(2,5\text{-}DMBT)_{12}Cl_4]^{2+}$: (A) Organization of clusters in a unit cell; (B) and (C) Packing diagrams along X and Y-axes, respectively display rectangular 2D lattice; (D) Packing diagram along Z-axis presents square 2D lattice; (E-G) The arrangement of ligands in $[Ag_{22}(dppe)_4(2,5\text{-}DMBT)_{12}Cl_4]^{2+}$ along x, y and z-axes.

Supporting information 14

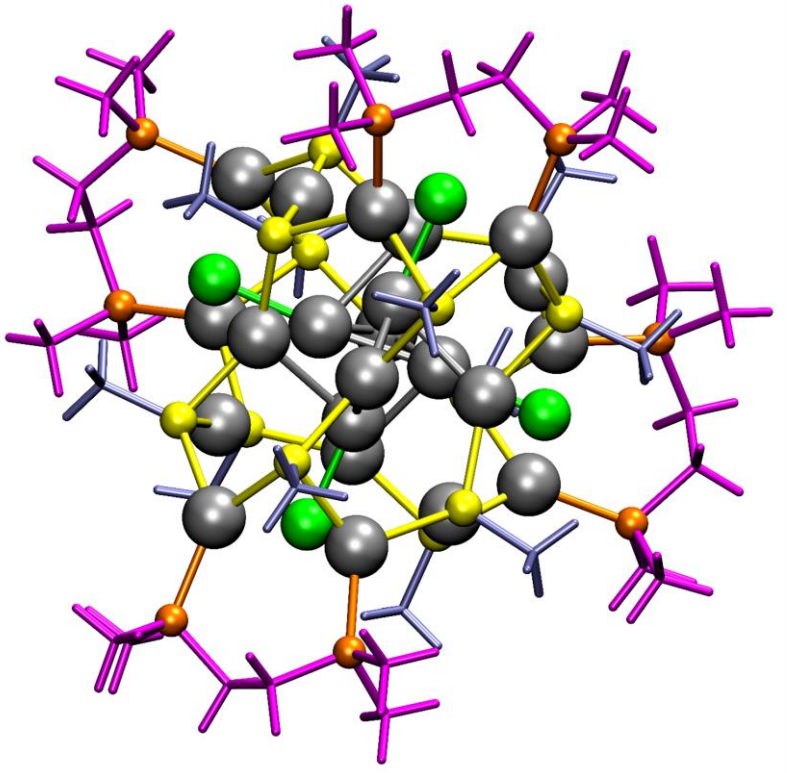

Figure S14. The reduced model structure, $[Ag_{22}(SMe)_{12}(Me_2PCH_2\text{-}CH_2PMe_2)_4Cl_4]^{2+}$ where benzene groups of each 2,5-DMBT and dppe were simplified using $-CH_3$ groups to reduce the cost of computation.

Supporting information 15

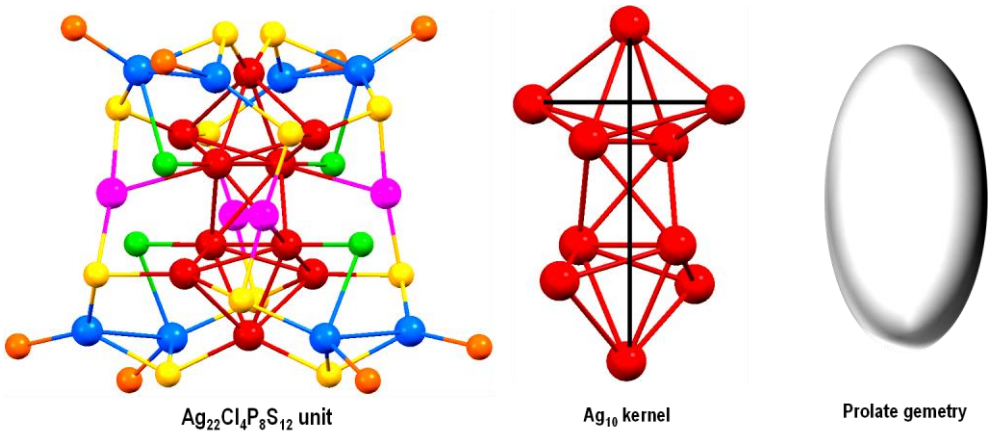

Figure S15. Schematic of the geometrical structure of the Ag_{10} core in $[Ag_{22}(dppe)_4(2,5\text{-}DMBT)_{12}Cl_4]^{2+}$ which possesses a prolate geometry.

Supporting information 16

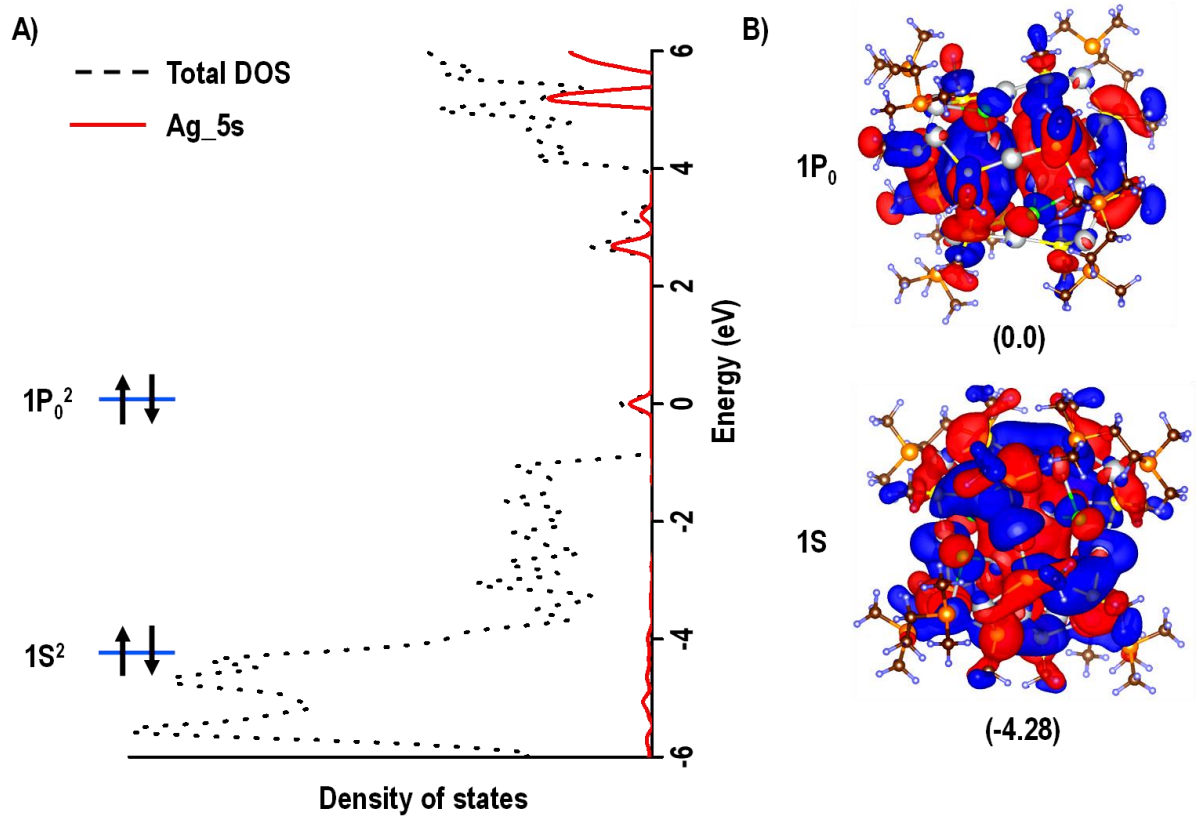

Figure S16. (A) Energy vs. density of states graph of $[Ag_{22}(dppe)_4(2,5\text{-}DMBT)_{12}Cl_4]^{2+}$ and the filling of 4e in the superatomic orbitals. (B) The isosurfaces of superatomic orbitals in $[Ag_{22}(dppe)_4(2,5\text{-}DMBT)_{12}Cl_4]^{2+}$. The highest molecular orbital is set to be at zero.

References

(1) Yang, H.; Lei, J.; Wu, B.; Wang, Y.; Zhou, M.; Xia, A.; Zheng, L.; Zheng, N. Crystal Structure of a Luminescent Thiolated Ag Nanocluster with an Octahedral Ag_6^{4+} Core. *Chem. Commun. (Cambridge, United Kingdom)* **2013**, *49*, 300–302.

(2) Shen, X.-T.; Ma, X.-L.; Ni, Q.-L.; Ma, M.-X.; Gui, L.-C.; Hou, C.; Hou, R.-B.; Wang, X.-J. $[Ag_{15}(N\text{-}Triphos)_4(Cl_4)](NO_3)_3$: A Stable Ag–P Superatom with Eight Electrons (N-Triphos = Tris((Diphenylphosphino)Methyl)Amine). *Nanoscale* **2018**, *10*, 515–519.

(3) Yang, H.; Wang, Y.; Zheng, N. Stabilizing Subnanometer Ag(0) Nanoclusters by Thiolate and Diphosphine Ligands and Their Crystal Structures. *Nanoscale* **2013**, *5*, 2674–2677.

(4) Dhayal, R. S.; Liao, J. H.; Liu, Y. C.; Chiang, M. H.; Kahlal, S.; Saillard, J. Y.; Liu, C. W. $Ag_{21}\{S_2P(OiPr)_2\}_{12}]^+$: An Eight-Electron Superatom. *Angew. Chemie - Int. Ed.* **2015**, *54*, 3702–3706.

(5) Liu, C.; Li, T.; Abroshan, H.; Li, Z.; Zhang, C.; Kim, H. J.; Li, G.; Jin, R. Chiral Ag_{23} Nanocluster with Open Shell Electronic Structure and Helical Face-Centered Cubic Framework. *Nat. Commun.* **2018**, *9*, 744.

(6) Joshi, C. P.; Bootharaju, M. S.; Alhilaly, M. J.; Bakr, O. M. $[Ag_{25}(SR)_{18}]^-$: The "Golden"Silver Nanoparticle Silver Nanoparticle. *J. Am. Chem. Soc.* **2015**, *137*, 11578–11581.

(7) AbdulHalim, L. G.; Bootharaju, M. S.; Tang, Q.; Del Gobbo, S.; AbdulHalim, R. G.; Eddaoudi, M.; Jiang, D.; Bakr, O. M. $Ag_{29}(BDT)_{12}(TPP)_4$: A Tetravalent Nanocluster. *J. Am. Chem. Soc.* **2015**, *137*, 11970–11975.

(8) Zou, X.; Jin, S.; Du, W.; Li, Y.; Li, P.; Wang, S.; Zhu, M. Multi-Ligand-Directed Synthesis of Chiral Silver Nanoclusters. *Nanoscale* **2017**, *9*, 16800–16805.

(9) Guan, Z. J.; Zeng, J. L.; Nan, Z. A.; Wan, X. K.; Lin, Y. M.; Wang, Q. M. Thiacalix[4]Arene: New Protection for Metal Nanoclusters. *Sci. Adv.* **2016**, *2*, 1–8.

(10) Yang, H.; Yan, J.; Wang, Y.; Su, H.; Gell, L.; Zhao, X.; Xu, C.; Teo, B. K.; Häkkinen, H.; Zheng, N. Embryonic Growth of Face-Center-Cubic Silver Nanoclusters Shaped in Nearly Perfect Half-Cubes and Cubes. *J. Am. Chem. Soc.* **2017**, *139*, 31–34.

(11) Bodiuzzaman, M.; Ghosh, A.; Shivan Sugi, K.; Nag, A.; Khatun, E.; Varghese, B.; Paramasivam, G.; Antharjanam, S.; Natarajan, G.; Pradeep, T. Camouflaging Structural Diversity: Co-Crystallization of Two Different Nanoparticles Having Different Cores but the Same Shell. *Angew. Chem. Int. Ed* **2018**, *57*, 1–7.

(12) Yang, H.; Wang, Y.; Huang, H.; Gell, L.; Lehtovaara, L.; Malola, S.; Häkkinen, H.; Zheng, N. All-Thiol-Stabilized Ag_{44} and $Au_{12}Ag_{32}$ Nanoparticles with Single-Crystal Structures. *Nat. Commun.* **2013**, *4*, 2422.

(13) Du, W.; Jin, S.; Xiong, L.; Chen, M.; Zhang, J.; Zou, X.; Pei, Y.; Wang, S.; Zhu, M. $Ag_{50}(Dppm)_6(SR)_{30}$ and Its Homologue $Au_xAg_{50-x}(Dppm)_6(SR)_{30}$ Alloy Nanocluster: Seeded Growth, Structure Determination, and Differences in Properties. *J. Am. Chem.*

Soc. **2017**, *139*, 1618–1624.

(14) Jin, S.; Wang, S.; Song, Y.; Zhou, M.; Zhong, J.; Zhang, J.; Xia, A.; Pei, Y.; Chen, M.; Li, P.; Zhu, M. Crystal Structure and Optical Properties of the $[Ag_{62}S_{12}(SBu^t)_{32}]^{2+}$ Nanocluster with a Complete Face-Centered Cubic Kernel. *J. Am. Chem. Soc.* **2014**, *136*, 15559–15565.

(15) Alhilaly, M. J.; Bootharaju, M. S.; Joshi, C. P.; Besong, T. M.; Emwas, A. H.; Juarez-Mosqueda, R.; Kaappa, S.; Malola, S.; Adil, K.; Shkurenko, A.; Häkkinen, H.; Eddaoudi, M.; Bakr, O. M. $[Ag_{67}(SPhMe_2)_{32}(PPh_3)_8]^{3+}$: Synthesis, Total Structure, and Optical Properties of a Large Box-Shaped Silver Nanocluster. *J. Am. Chem. Soc.* **2016**, *138*, 14727–14732.

(16) Yang, H.; Yan, J.; Wang, Y.; Deng, G.; Su, H.; Zhao, X.; Xu, C.; Teo, B. K.; Zheng, N. From Racemic Metal Nanoparticles to Optically Pure Enantiomers in One Pot. *J. Am. Chem. Soc.* **2017**, *139*, 16113–16116.

(17) Ren, L.; Yuan, P.; Su, H.; Malola, S.; Lin, S.; Tang, Z.; Teo, B. K.; Häkkinen, H.; Zheng, L.; Zheng, N. Bulky Surface Ligands Promote Surface Reactivities of $[Ag_{141}X_{12}(S\text{-}Adm)_{40}]^{3+}$ (X = Cl, Br, I) Nanoclusters: Models for Multiple-Twinned Nanoparticles. *J. Am. Chem. Soc.* **2017**, *139*, 13288–13291.

(18) Yang, H.; Wang, Y.; Chen, X.; Zhao, X.; Gu, L.; Huang, H.; Yan, J.; Xu, C.; Li, G.; Wu, J.; Edwards, A. J.; Dittrich, B.; Tang, Z.; Wang, D.; Lehtovaara, L.; Häkkinen, H.; Zheng, N. Plasmonic Twinned Silver Nanoparticles with Molecular Precision. *Nat. Commun.* **2016**, *7*, 12809.